Powerful Advanced N-Level Digital Architecture
for models of electrified vehicles and their components

https://project-panda.eu/

Research Innovation Action

GA # 824256

EUROPEAN COMMISSION
Horizon 2020 | GV-02-2018
Virtual product development and production of
all types of electrified vehicles and components

Deliverable No.	PANDA D3.1	
Deliverable Title	Multi-level knowledge models of e-drives	
Deliverable Date	2019-11-30	
Deliverable Type	REPORT	
Dissemination level	Public (PU)	
Written By	Mircea RUBA (UTCN), Calin HUSAR (SISW)	2019-10-10
Reviewed by	Walter LHOMME (ULille) Elena BREAZ (UBFC)	2019-11-20 2019-11-29
Approved by	Claudia MARTIS (UTCN) – WP3 leader	2019-11-25
Approved by	Alain BOUSCAYROL (ULille) - Coordinator	2019-11-29
Status	Final	2019-11-29

Publishable Executive Summary

Leader: Dr. Mircea RUBA (VUB), Participants: RTR, VEEM, SISW and UBFC

The objective of the project PANDA is to develop an open organization methodology for virtual and real testing of electrified vehicles. The present report details the accomplished research activities approached in WP 3, task 3.1. The focus in this task was to develop the multi-level models for the electrical machine under study. The targeted approach was to create simulation programs with 3 different complexity levels. The first one was designed to use constant parameters of the machine, the second one engaged look-up table based DQ inductance variations vs. currents while the most complex one, was based on 3D matrixes for the DQ flux variations vs the currents. All these studies were engaged on a known permanent magnet synchronous machine for which the complete identification and design data is available. The created models can be easily modified to become self-exited synchronous machine models. The simulations prove the functionality of the models and the difference in results highlight the more realistic behavior of the flux linkage-based model versus the one with constant DQ inductances. The cooperation with Siemens Industry Software engaged the transition of the models from Matlab Simulink to Simcenter Amesim using its new EMR library. Preliminary Amesim based simulations prove the functionality of the models as well as those in Matlab Simulink. The future investigations scheduled for task 3.2 and 3.4 are focused for the multi-level analysis of the inverter and then HiL validation of the complete e-drive models vs. measured laboratory data.

Contributions:

No	*Who*	*Description*	*Date*
1	UTCN	D3.1 report creation and outline	2019-07-01
2	UTCN	Section 1, 2	2019-08-01
3	UTCN	Section 3	2019-09-01
4	UTCN	Section 4	2019-10-01
5	SISW	Section 5	2019-10-01
6	UTCN	Update and conclusion	2019-11-28

Contents

1. Introduction....5
2. Finite element analysis of the AC machine 6
   2.1. AC machine selection....6
   2.2. Permanent magnet synchronous machine under study....7
      2.2.1. First level analysis of the PMSM 7
      2.2.2. Second level analysis of the PMSM using Frozen Permeability method 9
      2.2.3. Third level analysis of the PMSM using flux and torque maps 10
3. Development of the e-drive model in MATLAB/Simulink 13
   3.1. Development of the simulation models of the e-drive using MATLAB/Simulink 14
4. Simulation results....18
5. Development of the E-drive model in Simcenter AMESim using EMR....21
   5.1. Simcenter AMESim Electric Motors and Drives (EMD) Library....21
   5.1.1. Library content 21
   5.1.1.1. Category structure....21
   5.1.1.2. Notations and conventions 22
   5.1.1.2.1. Electrical conventions: dipoles....22
   5.1.1.2.2. Electrical conventions: three phase windings....23
   5.1.1.2.3. Electrical conventions: electrical angle 23
   5.1.1.2.4. Space phasor definition 23
   5.1.1.2.5. Mechanical convention....24
   5.2. EMR-based e-drive in Simcenter AMESim 24
6. Conclusions and future work....30
7. Deviations....31
8. References....31

Appendix A – Project Partners 32
Appendix B – EMR graphical pictogram 33
Appendix C - Abbreviations....34

List of figures

Figure 1. Cross-section of the 2.5 kW PMSM 6
Figure 2. The inductance measurement circuit....8
Figure 3. The current step response for the determination of Lq inductance 8
Figure 4. Ld and Lqd inductances extracted from Frozen Permeability simulation 9
Figure 5. Lq and Ldq inductances extracted from Frozen Permeability simulation 10
Figure 6. Original flux linkage map for d-axis 11
Figure 7. Original flux linkage map for q-axis 11
Figure 8. Electromagnetic torque map....11
Figure 9. Inverse flux linkage maps for d-axis 12
Figure 10. Inverse flux linkage maps for q-axis 12
Figure 11. The EMR representation of the e-drive model 13
Figure 12. Tunning path of the e-drive model 14
Figure 13. Screenshot of the e-drive model from MATLAB/Simulink 14
Figure 14. Configuration of the three-phase inverter circuit. 15
Figure 15. Block diagram of the PMSM windings....16
Figure 16. The block diagram for the flux linkage model 18
Figure 17. The dq components of the flux for the PMSM 19
Figure 18. The dq components for the back e.m.f for the PMSM 19
Figure 19. The speed of the PMSM 20
Figure 20. The electromagnetic torque of the PMSM....20
Figure 21. EMD library structure 21
Figure 22. EMD library content 22
Figure 24. Electrical angle definition 23
Figure 25. Space phasor representation 24
Figure 26. The mechanical convention definition 24

List of Tables

Table 1. PMSM 2.5kW main data 7
Table 2. Electrical convention for current and voltage 22
Table 3: Winding connection and electrical convention for three-phase machines....23
Table 4: Project Partners....32
Table 5: EMR pictogram [Bouscayrol 2012] 33

1. Introduction

The project PANDA aims to propose an open general framework for seamless integration of models for virtual and real testing of electrified vehicles. This global framework will enable a smart reuse of the models in the different parts of a W-model leading to reduce time and increase reliability. To achieve this goal, in WP3, a multi-scale multi-domain models of e-drives according to the PANDA methodology will be provided. In this report, the development of the multi-level knowledge model for the AC machine is described.

The goal of the WP3 is to develop three complexity levels models of an AC electric machine for e-drive. The model comprises the machine under test, its converter and the control unit. In the simulation, an ideal model for the converter and the control unit based on indirect field-oriented control (FOC) are considered. Further investigations are made after the validation of the propulsion system. The developed modelling method are transferred into an industrial software package known as AMESim, using the dedicated functional causal library based on the WP1 approach.

First, the selected AC machine to be studied under WP3 are defined. Then, a finite element analysis (FEA) of the machine is performed in order to evaluate its electromagnetic behaviour and perform the parameter computation. The analysis considers 3 levels of complexity; therefore, several simulations are performed in Flux Skew environment in order to extract the following data:

- Constant values for the machine parameters will be considered for the first level of complexity;
- Look-up tables for describing the variation of the machine inductances, computed via FEA based on frozen permeability procedure, considering only the saturation phenomenon;
- Look-up tables for DQ fluxes and developed electromagnetic torque, extracted from FEA, considering both saturation and cross-saturation phenomena.

Once the parameters are computed the e-drive models is implemented in MATLAB/Simulink environment.

The general scope of work presented in this report is focused on creating flexible and reliable multi-level models for the synchronous machine, in particular for the permanent magnet excited (PMSM) one. However, transitioning from this machine to the classical electromagnetically excited synchronous machine is only matter of replacing the permanent magnet flux with the one calculated in the rotor. The choice of developing these models for the PMSM was considered as the team from UTCN have at their disposal all the detailed data of such a machine as well as their laboratory owns the actual machine.
The multi-level analysis of the electronic power inverter, quantifying the switching losses are starting tasks that will be part of the T3.2, while the complete experimental validation of the PMSM models as well as the ones of the power inverter will be approached in T3.4, HiL testing.

2. Finite element analysis of the AC machine

2.1. AC machine selection

The goal of WP3 is to provide different multi-scale multi-domain models of e-drives according to the WP1 unified method. These models will be developed and validated for a 2.5 kW permanent magnet synchronous machine (PMSM) .

After the validation, the methodologies will be applied for testing of both virtual and real propulsion systems of the vehicles considered in PANDA. This can be done by using scaling methods [Nemes, 2019]:

1) 65 kW self excitation synchronous machine based propulsion system of a BEV (Battery Electrical Vehicle) provided by Renault Technologie Roumanie (RTR). Measured data of the propulsion system of a Renault Zoe for different driving scenarios is available. The virtual testing will be compared with the previous development.
2) 6 kW PMSM based propulsion system of a light Fuel Cell Vehicle (FCV) developed in the frame of FP7 MobyPost project, provided by UBFC. All parameters and Fuel Cell test bench are available, as wel as some driving tests. The virtual testing will be compared with the previous development.
3) 6 kW PMSM based propulsion system of an innovative Plug-in Hybrid Electric Vehicle (P-HEV), based on a demo car of Valeo (VEEM). A series-parallel HEV with a 48V battery and low-voltage electrical machines will be considered. The new electrical subsystems (batteries and e-drive) will be studied both in virtual and real testing

For the development of WP3 methodology and its characterization a 2.5 kW PMSM with the cross-section presented in Figure 1 will be considered.

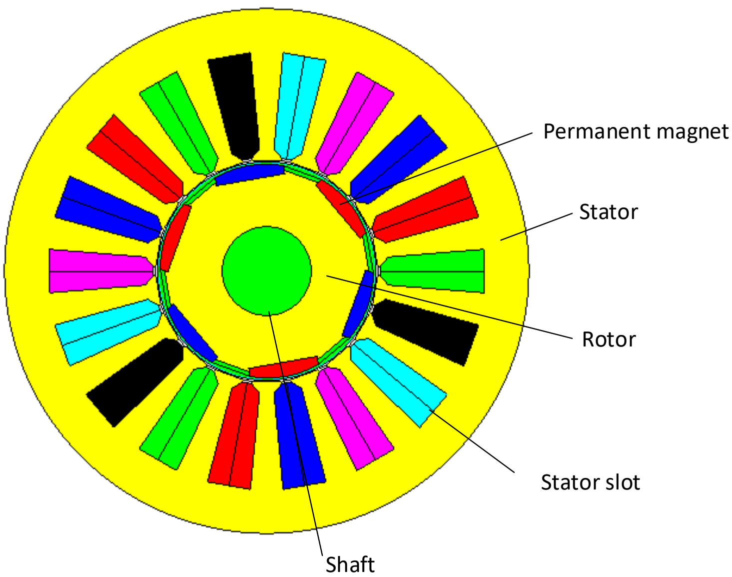

Figure 1. Cross-section of the 2.5 kW PMSM

2.2. Permanent magnet synchronous machine under study

The characterization of the machine was performed using a dedicated software environment, Flux Skew. The main constructive data of the machine under study is reported in Table 1.

Table 1. PMSM 2.5kW main data

	Dimension	**Value**	**Unit**
1	Stator slots	18	-
2	Number of phases	3	-
3	Winding configuration	Double Layer	-
4	Winding connection	Star-connection	-
5	Number turns on the phase	48	-
6	Type of winding	Distributed	-
7	Length of the machine	160	[mm]
8	Diameter of the machine	118	[mm]
9	Rated speed	2000	[rot/min]
10	Frequency	100	[Hz]
11	Phase resistance	0.2	[Ω]
12	Torque at rated current	12	[Nm]
13	Rated current per phase	21	[A]
14	Mechanical power	2500	[W]
15	DC Voltage link	120	[V]
16	Magnet material	Sintered NdFeb N35SH_20DEG	-
17	Stator and rotor core	Steel M530_50A_50HZ	-
18	Windings material	FLU_COPPER	-

2.2.1. First level analysis of the PMSM

For the first level analysis the saturation of the PMSM is neglected. The machine inductances are computed using an experimental-based approach. For the circuit presented in Figure 2 a voltage pulse is applied and the current response is analysed (Figure 3) [Bobek, 2005].

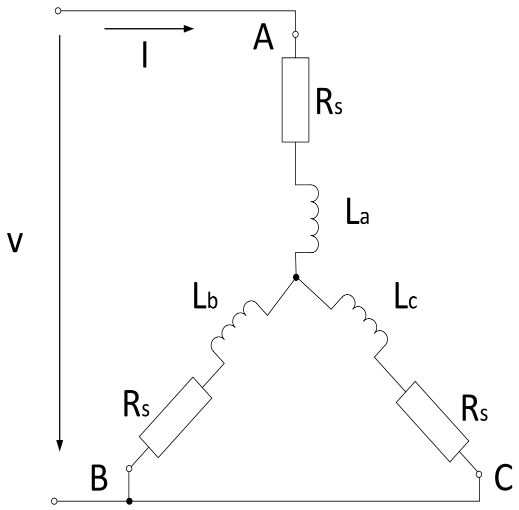

Figure 2. The inductance measurement circuit

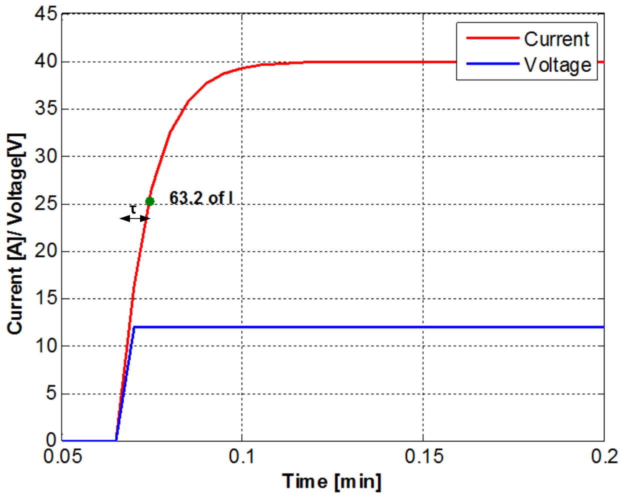

Figure 3. The current step response for the determination of Lq inductance

In order to estimate the d-axis inductance phase A is aligned with the d-axis of the rotor and connected to the positive terminal. With phase B and C grounded, a negative step voltage is applied, and the current is measured. The electric constant of the circuit is given by:

$$\tau = \frac{L}{R} \tag{1}$$

for:

$$I_\tau = 63.2\% \cdot I \tag{2}$$

and R as:

$$R_s = 0.2[\Omega] \tag{3}$$

The d-axis inductance results as:

$$L_d = \frac{2}{3} \cdot L \quad (\theta_{el} = 0^\circ) \tag{4}$$

The estimation of the q-axis inductance the same approach is used, but applying a positive step voltage. Thus, the current is measured, and the inductance can be calculated using (1), (2) and (5).
As expected, d- and q-axis inductances are equal:

$$L_q = \frac{2}{3} \cdot L \quad (\theta_{el} = 90^\circ) \tag{5}$$

$$L_d = L_q = 0.002817\,[H] \tag{6}$$

2.2.2. Second level analysis of the PMSM using Frozen Permeability method

This method assumes that the permanent magnets (PMs) of the PMSM are frozen, meaning that the PM flux is turned off by setting the PM remanence to zero. This is the most effective approach to calculate the saturated inductances Ld and Lq and the mutual inductances Ldq, Lqd. The method considers the magnetic saturation, therefore the Ld and Lq can be calculated as function of the currents d and q [Zarko, 2005].
Once the permeabilities are frozen the problem becomes linear and the parameters can be determined. Four magnetostatics simulations are needed in order to determine the four inductances.
In order to compute Ld and Lqd the PM flux is turned off by setting the remanence Br to zero and the current vector is aligned with the d axis. Simulations are performed for 55 values of d-axis current between -200A and 200 A. The q-axis current is zero. Based on phase linkage fluxes, d- and q- axis fluxes are computed as:

$$\Psi_d = \frac{2}{3}(\Psi_a - \frac{1}{2}\Psi_b - \frac{1}{2}\Psi_c) \tag{7}$$

$$\Psi_q = \frac{1}{\sqrt{3}}(\Psi_b - \Psi_c) \tag{8}$$

The d and qd inductances result as:

$$L_d = \frac{\Psi_d}{i_d} \tag{9}$$

$$L_{qd} = \frac{\Psi_q}{i_d} \tag{10}$$

with the shape depicted in Figure 4.

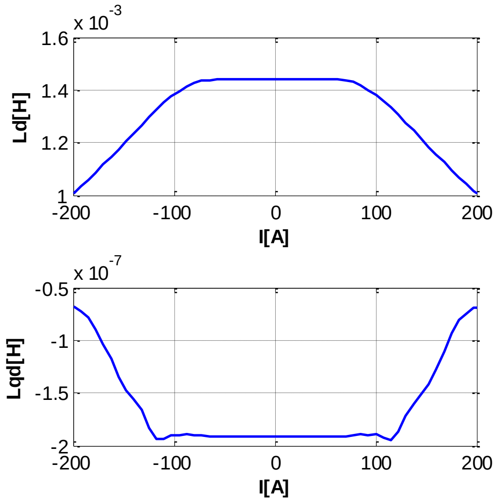

Figure 4. Ld and Lqd inductances extracted from Frozen Permeability simulation

The inductances Lq and Ldq are computed using a similar approach, the only difference is that the current vector it's aligned with the q axis. Simulations are performed for 55 values of q-axis current between -200A and 200 A, while d-axis current is set to zero. D- and q-axis fluxes are computed and thus, the inductances result as:

$$L_q = \frac{\Psi_q}{i_q} \tag{11}$$

$$L_{dq} = \frac{\Psi_d}{i_q} \tag{12}$$

They are depicted in Figure 5.

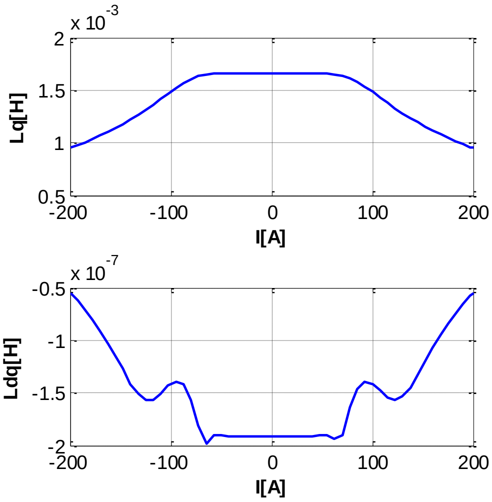

Figure 5. Lq and Ldq inductances extracted from Frozen Permeability simulation

In Figure 4 and 5 I stands for the id and iq currents, both having equal values.
It can be noticed that the saturation phenomena result in inductances dependence on d- and q-axis currents, respectively.

2.2.3. Third level analysis of the PMSM using flux and torque maps

Flux linkage model (FLM) brings a higher accuracy as it includes both saturation and cross-saturation phenomena. FEA is performed for different values of d- and q-axis between -200 A and 200 A, for current vector alignment with d- and q-axis, respectively. Flux-linkages and electromagnetic torque maps are extracted [Drobnic, 2019].

Figure 6 and 7 shows the flux-linkage maps for the PMSM. A high nonlinearity can be noticed for both d- and q-axis flux linkage. For d-axis flux-linkage (Figure 6) the surface curvature along d-axis represents the main saturation, whereas the curvature along the q axis (Figure 7) indicates the cross-saturation. Figure 8 depicts the electromagnetic torque of the PMSM as function of d- and q-axis. The nonlinear effect is higher for higher d- and q-axis currents.

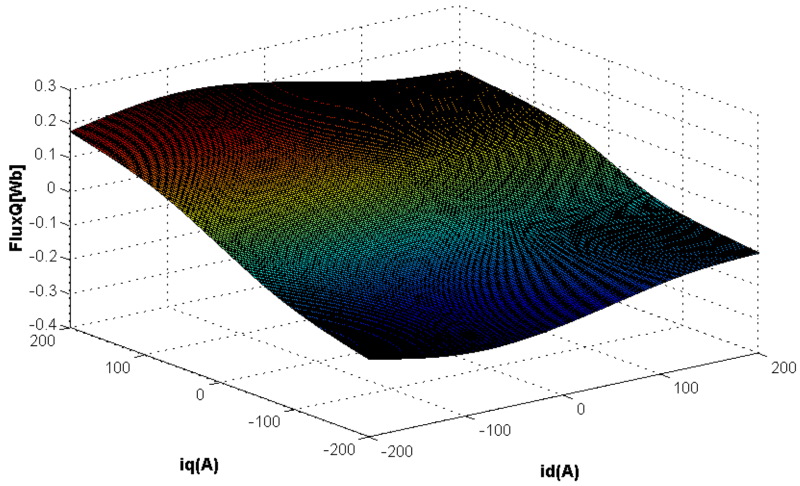

Figure 6. Original flux linkage map for d-axis

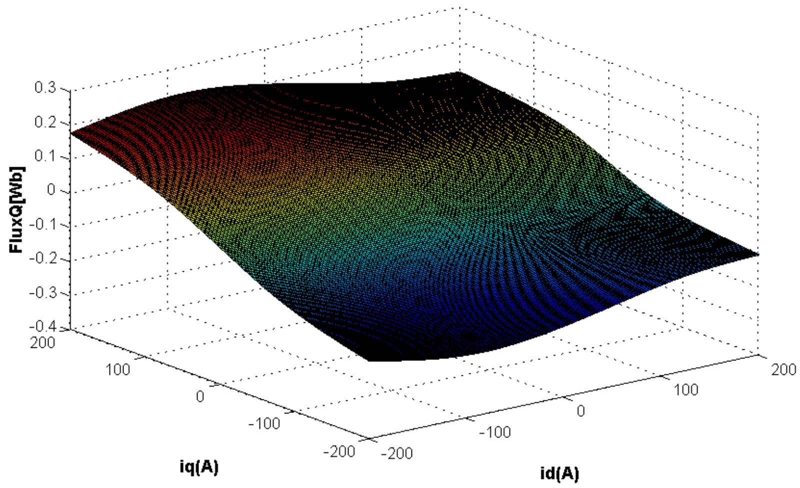

Figure 7. Original flux linkage map for q-axis

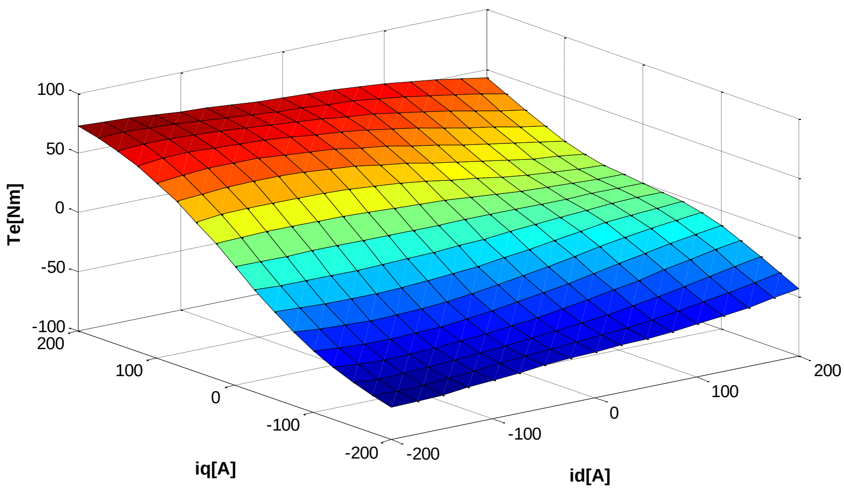

Figure 8. Electromagnetic torque map

For the implementation of the state-space equations based model a current-flux relation has to be defined:

$$i = g(\Psi) \tag{13}$$

In order to realize the inversion of the flux-linkage maps the corresponding interpolating functions are defined:

$$i_d = g_d(\Psi_d, \Psi_q) \tag{14}$$

$$i_q = g_q(\Psi_d, \Psi_q) \tag{15}$$

The solution to determine the inverse map id and iq is via intersection [Pinto, 2017]. The original flux linkage maps Ψd and Ψq are first interpolated and sliced into predefined number of contours isolines at the new flux-linkage levels Ψd and Ψq. These lines can be defined as curves in the current coordinates, where each of these curves codify all possible combinations (id, iq) for a flux-linkage level. The intersection algorithm proceeds to find an intersection between curves at Ψd and Ψq for all combinations of the stator flux linkage. The resulting new flux linkage maps can be seen in Figures 9 and 10.

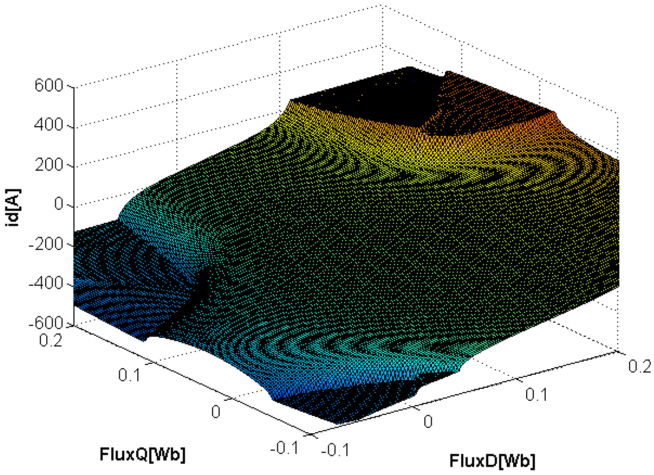

Figure 9. Inverse flux linkage maps for d-axis

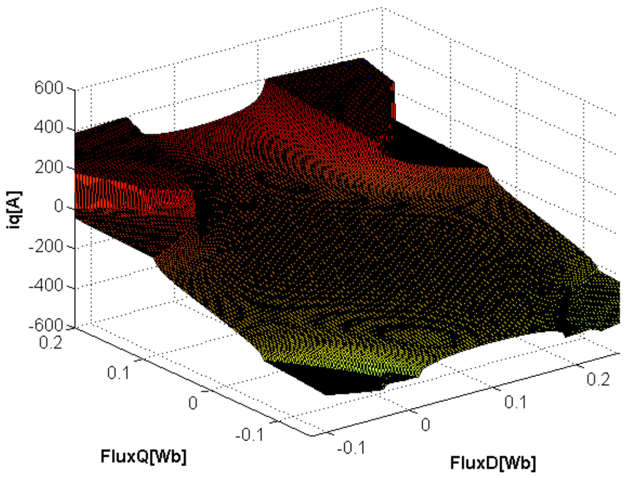

Figure 10. Inverse flux linkage maps for q-axis

All the results obtained from FEA are exported as look-up-tables in order to be used further for dynamic simulation.

3. Development of the e-drive model in MATLAB/Simulink

The e-drive model integrates the machine model (based on one of the above described assumptions), a simplified model of the voltage source inverter (VSI) and the control unit, based on indirect field-oriented control (FOC).

All the models are built in MATLAB/Simulink using the energetic macroscopic representation (EMR), according to the PANDA methodology. Energetic Macroscopic Representation (EMR) is a graphical description, which highlights energy properties of the system. It organizes the system into interconnected basic elements: source of energy (green oval), adaptation of energy (orange square with a triangle inside), accumulation of energy (orange crossed rectangle), monodomain (orange square) or multidomain conversion (orange circle), and distribution of energy (double orange square) [LHomme, 2012], [Bouscayrol 2012].

The EMR has been developed in order to propose a synthetic and dynamical description of electromechanical conversion systems. Using EMR, brings in the novelty of standardized simulation model architectures. This description allows the subdivision of the whole complex system into simple blocks, which yields a synthetic and physical representation based on the causality principle and the action and reaction principle. The product of the action and reaction variables, which link both elements, leads to the instantaneous power exchanged. Furthermore, all the components are described respecting the integral causality [Bouscayrol, 2012]. This way, wrong connection of the simulation subsystems is completely diminished. Also, facilitates reusing and understanding of the models by any researcher that has EMR skills.

In Figure 11 the complete EMR diagram of the e-drive is shown. The system contains the electrical source, the 3-Voltage Source Inverter (VSI) and the machine under test with a mechanical shaft and a mechanical load. The e-drive model is developed using EMR (orange pictograms) then the whole control structure is obtained, using inversion rules (blue pictograms). In order to obtain the required estimators, parts of the EMR system model can be reused. Thus, the purple estimation blocks of Figure 11 are introduced by reusing the model equations.

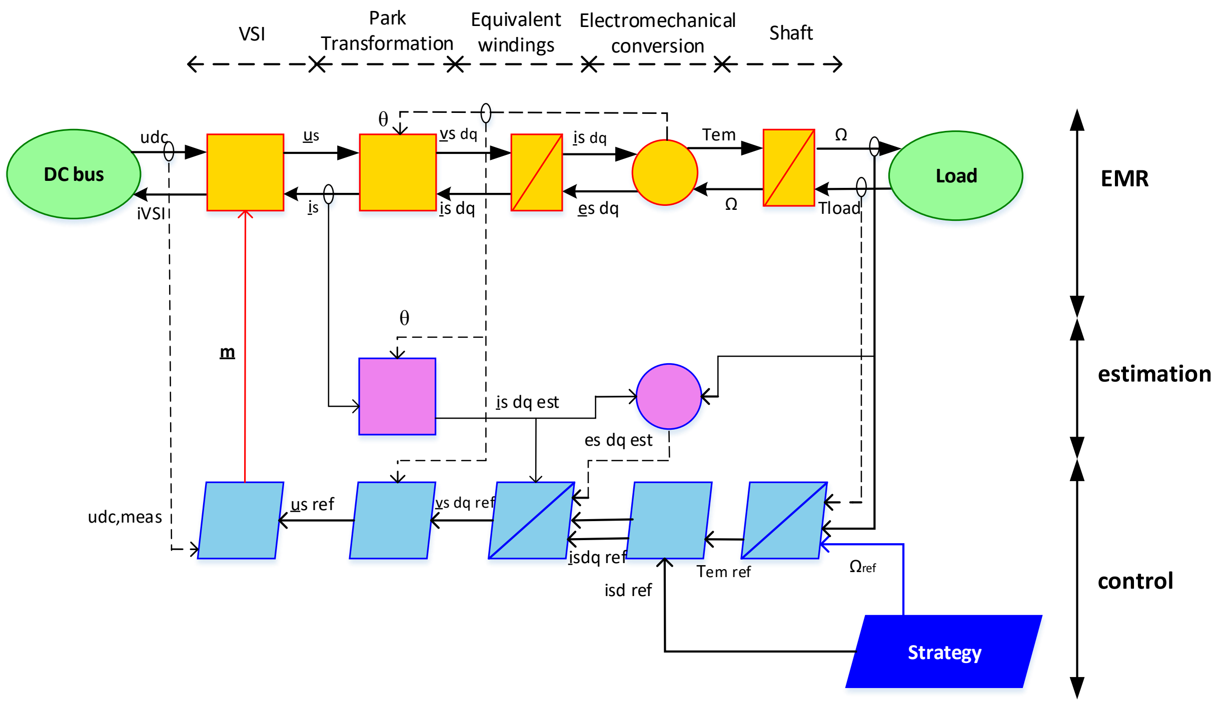

Figure 11. The EMR representation of the e-drive model

The tuning path is defined from the tuning input chosen to act on the system to the output variable to control. The suitable tuning input is clearly the modulation function of the inverter m while the output to control is the angular speed Ω of the machine. The tuning path is depicted below in Figure 12.

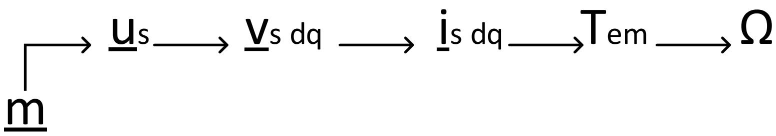

Figure 12. Tunning path of the e-drive model

Three EMR models are implemented in MATLAB/Simulink using the three levels of machine characterization accuracy. The analytical models have different complexities: the first one is the ideal dq model where all the parameters of the machine are constant; the second integrates the saturation phenomenon, and the machine inductances are defined as look-up tables according to the currents; the third one takes into account both saturation and cross-saturation phenomena, defining d- and q- axis fluxes, as well as the electromagnetic torque as functions of both d- and q-axis currents.

3.1. Development of the simulation models of the e-drive using MATLAB/Simulink

Figure 13 presents a screenshot of the e-drive EMR model implemented in MATLAB/Simulink from the library developed by Univ. Lille [EMR 2019].

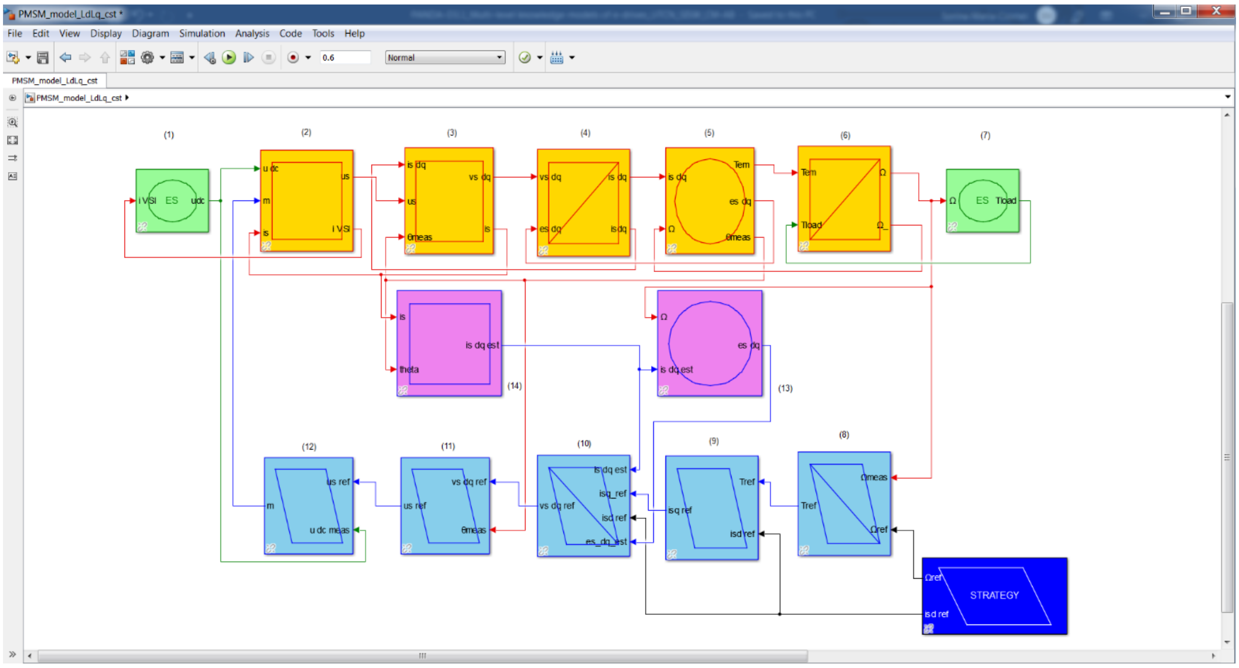

Figure 13. Screenshot of the e-drive model from MATLAB/Simulink

The DC bus block (1) imposes the inverter's capacitor voltage at 120 V. The block is represented by a source EMR element.
The second block represents the three-phase voltage source inverter (VSI) based on the received three-phase PWM signals (m). It is represented by a conversion element. The EMR element convert energy without storage and therefore their outputs and inputs are not defined before connection to other elements. A configuration of the three-phase VSI can be seen in Figure 14.
The Sinusoidal Pulse Width Modulation (SPWM) technique treats each modulating voltage as a separate entity that is compared to the common carrier triangular waveform. The three-phase voltage set of variable amplitude is compared in three separate comparators with a common *triangular carrier waveform of fixed amplitude*. The PWM a, b, c values are 0 or 1 as the output of the comparators (*m*) signal imposes it.

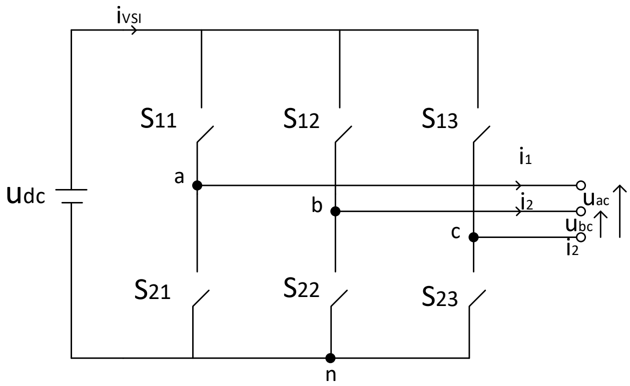

Figure 14. Configuration of the three-phase inverter circuit.

$$u_{DC} = 120\,[V] \tag{16}$$

$$u_s = [u_{ac} \;\; u_{bc}]^T \tag{17}$$

$$i_s = [i_1 \;\; i_2]^T \tag{18}$$

The relationship between the line-to-negative voltages and the switching states are:

$$v_{an} = S_{11} \cdot u_{dc} \tag{19}$$

$$v_{bn} = S_{12} \cdot u_{dc} \tag{20}$$

$$v_{cn} = S_{13} \cdot u_{dc} \tag{21}$$

The relationship between the line-to-line voltages and the switching states are [Delarue 2003]:

$$v_{ac} = v_{an} - v_{cn} = (S_{11} - S_{13}) \cdot u_{dc} \tag{22}$$

$$v_{bc} = v_{bn} - v_{cn} = (S_{12} - S_{13}) \cdot u_{dc} \tag{23}$$

$$\underline{u}_s = \underline{m} \cdot u_{dc} \tag{24}$$

$$i_{VSI} = \underline{m}^T \cdot \underline{i}_s \tag{25}$$

The voltages used to calculate the dq voltages are :

$$\begin{pmatrix} v_{ak} \\ v_{bk} \\ v_{ck} \end{pmatrix} = \frac{1}{3} \begin{pmatrix} 2 & -1 \\ -1 & 2 \\ -1 & -1 \end{pmatrix} \cdot \begin{pmatrix} u_{ac} \\ u_{bc} \end{pmatrix} \tag{26}$$

Where k is considered fictitious neutral.

The 3-phase reference frame is converted using Park transformation to a 2-axis reference frame (third block, conversion element). This allows the implementation of the indirect field-oriented control strategy.
The objective is to control the direct and quadrature-axis current id and iq to achieve the reference speed. The dq model of the machine windings are detailed in block (4) and the corresponding block diagram is shown in Figure 15.
The stator voltage equation can be transformed into dq coordinates, yielding the d and q components as:

$$v_{sd} = R_s \cdot i_{sd} + \frac{d}{dt}\psi_{ds} - \omega \cdot \psi_{qs} \tag{27}$$

$$v_{sq} = R_s \cdot i_{sq} + \frac{d}{dt}\psi_{qs} + \omega \cdot \psi_{ds} \tag{28}$$

The basic flux equations of a PMSM are implemented in block (5):

$$\frac{d}{dt}\psi_{ds} = v_{sd} - R_s \cdot i_{sd} - e_{sd} \tag{29}$$

$$\frac{d}{dt}\psi_{qs} = v_{sq} - R_s \cdot i_{sq} - e_{sq} \tag{30}$$

The back electromotive force (emf) equation (eq. 31 and 32) and the corresponding electromechanical conversion given by the torque equation (eq. 39) are represented by a conversion element (block number 5).

$$e_{sd} = -\omega \cdot \Psi_{qs} \tag{31}$$

$$e_{sq} = \omega \cdot \Psi_{ds} \tag{32}$$

$$\Psi_{ds} = \Psi_{md} + L_d \cdot I_{ds} + L_{dq} \cdot I_{qs} \tag{33}$$

$$\Psi_{qs} = \Psi_{mqd} + L_q \cdot I_{qs} + L_{qd} \cdot I_{ds} \tag{34}$$

$$\frac{d}{dt}\psi_{ds} = \frac{d}{dt}\psi_{md} + L_d \cdot \frac{d}{dt} i_{ds} + L_{dq} \cdot \frac{d}{dt} i_{qs} \tag{35}$$

$$\frac{d}{dt}\psi_{qs} = \frac{d}{dt}\psi_{mqd} + L_q \cdot \frac{d}{dt} i_{qs} + L_{qd} \cdot \frac{d}{dt} i_{ds} \tag{36}$$

$$L_d \cdot \frac{d}{dt} i_{ds} = v_{sd} - R_s \cdot i_{sd} - e_{sd} - L_{dq} \cdot \frac{d}{dt} i_{qs} \tag{37}$$

$$L_q \cdot \frac{d}{dt} i_{qs} = v_{sq} - R_s \cdot i_{sq} - e_{sq} - L_{dq} \cdot \frac{d}{dt} i_{qs} \tag{38}$$

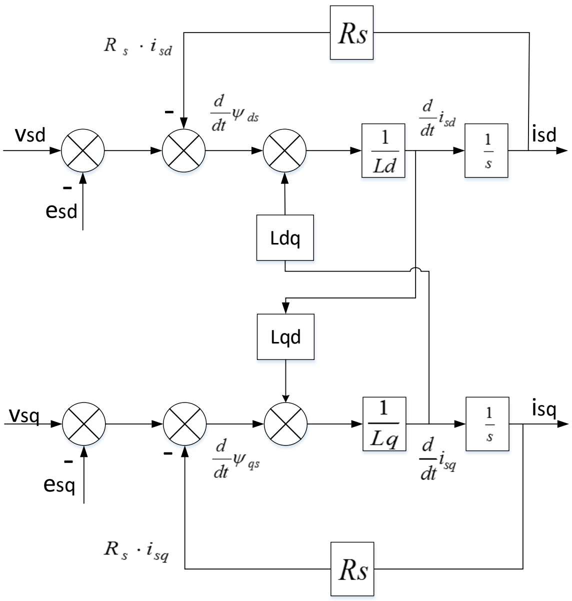

Figure 15. Block diagram of the PMSM windings

$$T_{em} = \frac{3}{2} \cdot p \cdot (\Psi_{ds} \cdot i_{qs} - \Psi_{qs} \cdot i_{ds}) \tag{39}$$

$$\omega = \Omega \cdot p \tag{40}$$

In the above equations Ψ_{md} represent the PM flux, ω is the angular velocity of the machine and p the number of poles pairs.

The sixth block, represented by an accumulation element corresponds to the mathematical conversion defined by the electromagnetic torque produced by the PMSM, the load torque, the moment of inertia denoted by J and the friction coefficient B.

$$J \frac{d\Omega}{dt} = T_{em} - T_{load} - B \cdot \Omega \tag{41}$$

In order to implement the control strategy some parameters need to be estimate.

The values for the dq components for the back emf are estimated in block no. 13 which is represented by a conversion EMR element.

$$e_{sd\_est} = -\Psi_{qs} \cdot \omega \tag{42}$$

$$e_{sq\_est} = \Psi_{ds} \cdot \omega \tag{43}$$

The machine currents idq are obtained by performing the inverse Park transformations that can be seen in block (14). The equation is represented by an EMR conversion element with an additional input of the dq transformation angle θ.
The control strategy is implemented using inversion-based control, therefore from reaction to action the EMR control architecture is built. Being a three-phase machine, the PMSM is controlled with the classical field-oriented control (FOC), function of the phase currents in dq representation and of the rotor position.

$$i_{sq\_ref} = \frac{T_{pmsm}}{\frac{3}{2} \cdot p \cdot \left[\Psi_{md} + \left(L_{sd} - L_{sq}\right) \cdot i_{sd}\right]} \tag{44}$$

$$i_{sd\_ref} = 0 \tag{45}$$

There are three PI regulators in the control system. One is for the mechanical system (speed) computed in block no. 8 and 9 and two are for the electrical system (d and q currents) represented in block no. 10. Speed controller calculates the difference between the reference speed and the actual speed producing an error, which is fed to the PI controller. This regulator outputs the reference current isq function of the reference torque.
The gain for the regulators were computed using Ziegler-Nichols tuning method and later were manually fine-tuned for a better response [Yucelen, 2016].
Using the measured dq currents, the estimated dq back emf voltages and two PI regulators, the dq voltages are computed.
The dq reference voltages need to be transformed using the reverse Park transformation into 3-phase quantities for SPWM modulation to obtain the gate signals to feed the inverter. In three-phase SPWM, a PWM carrier (vtr), set at frequency of 10 [kHz], is compared with three sinusoidal control voltages us a,b,c. The output of the comparison will be 0 or 1 and these values will represent in fact the states of the switches.
The last simulation model that was implemented in this paper is the most complex and accurate as it uses the fluxes and the torque extracted from the FEA and introduce them via look-up tables in the block diagram from Figure 16.

$$i_{sd} = h(\Psi_{sd}, \Psi_{sq}) \tag{46}$$

$$i_{sq} = h(\Psi_{sd}, \Psi_{sq}) \tag{47}$$

$$T_{em} = h(i_{sd}, i_{sq}) \tag{48}$$

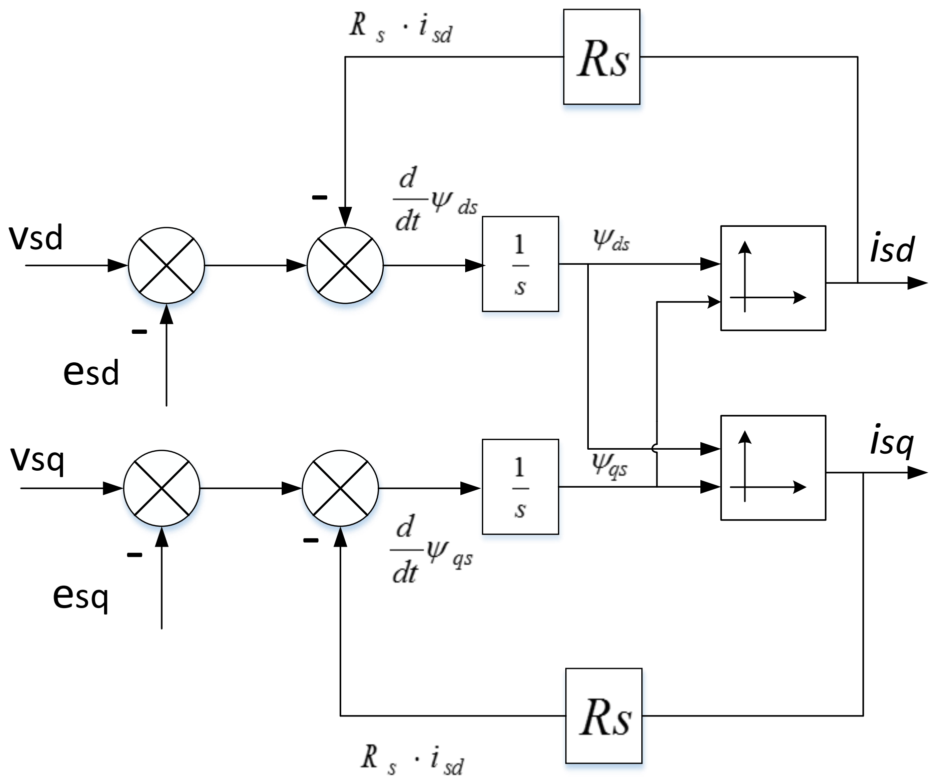

Figure 16. The block diagram for the flux linkage model

4. Simulation results

In order to test the three models of the PMSM a reference speed of 210 rad/s, equal to the rated one, a reference load of 24 Nm, which is the load torque Tload, are considered for simulation. The scope of work during simulation results analysis is to observe the behavior of the machine excited by the same inputs. The results at this level will be discussed without any comparison to experimental results. The latter will be approached during T3.4.
It can be observed in Figure 17 that for the first level model in which all the parameters of the PMSM are constant values, reaches the highest magnetic flux because this model does not take into account the saturation. For the same test condition, the flux linkage model highlights the influence of the saturation, as the inductances on the DQ axis were fetched from FEA modelling. There is a consistent difference between the results for the studied conditions. In considering the DQ inductances constant, the model becomes more ideal, while considering material saturation, the results are closer to real behavior.

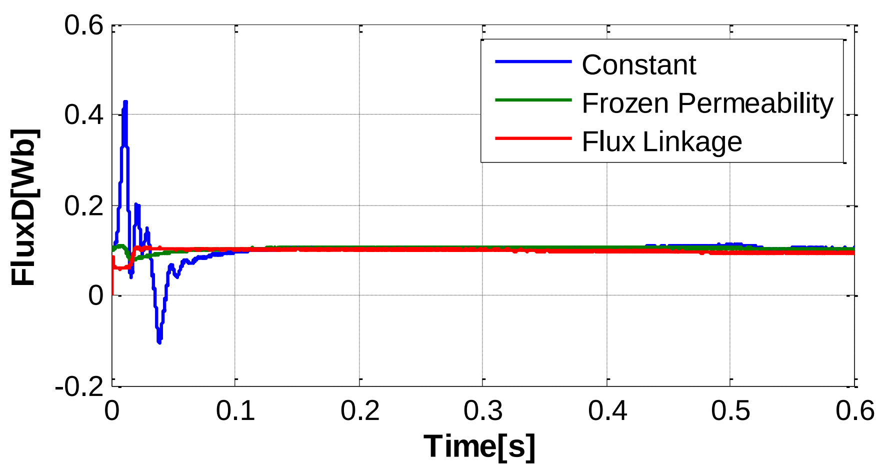

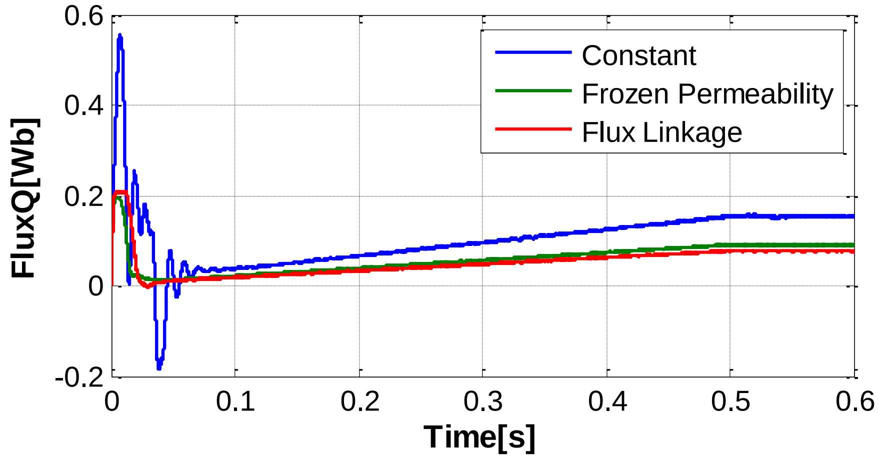

Figure 17. The dq components of the flux for the PMSM

In Figure 18 it is shown the back electromotive force of the PMSM from the three simulation models. The back emf is proportional to the speed of the motor, therefore it increases with it. Actually, the variation of the back emf is a replica of the machine velocity, reaching maximum values when the speed reaches rated values.

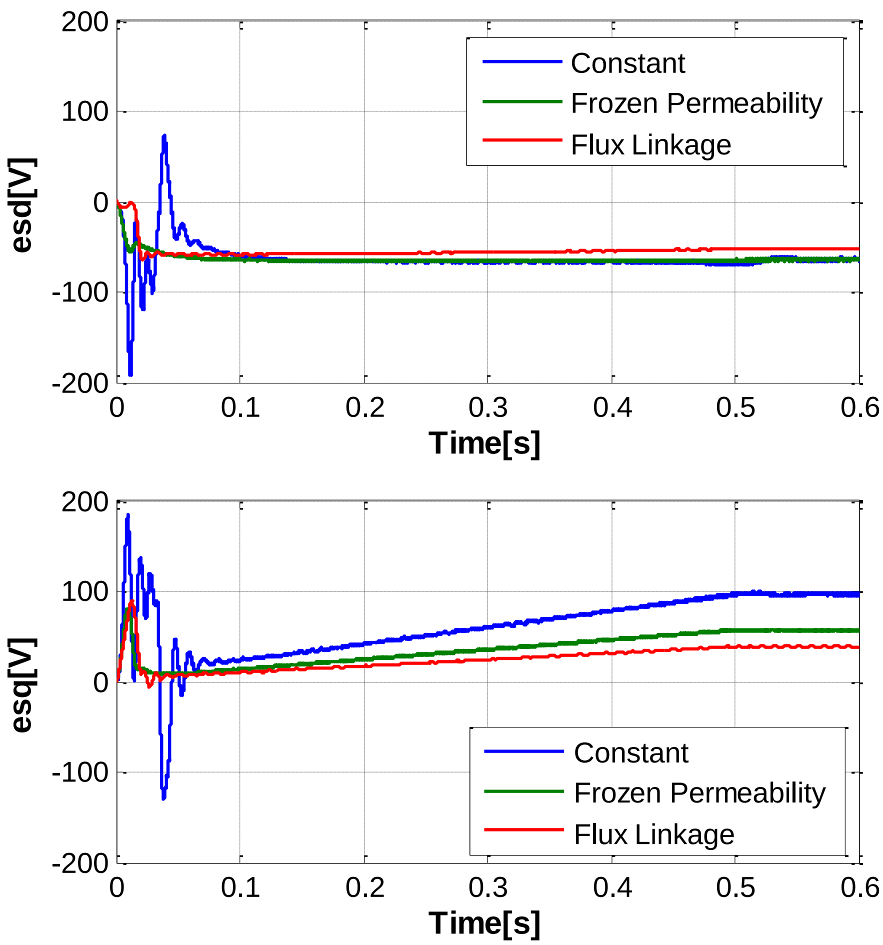

Figure 18. The dq components for the back e.m.f for the PMSM

A 200 rad/s was given as a reference speed, as shown in Figure 19. It can be seen that all the three models are able to follow the reference.

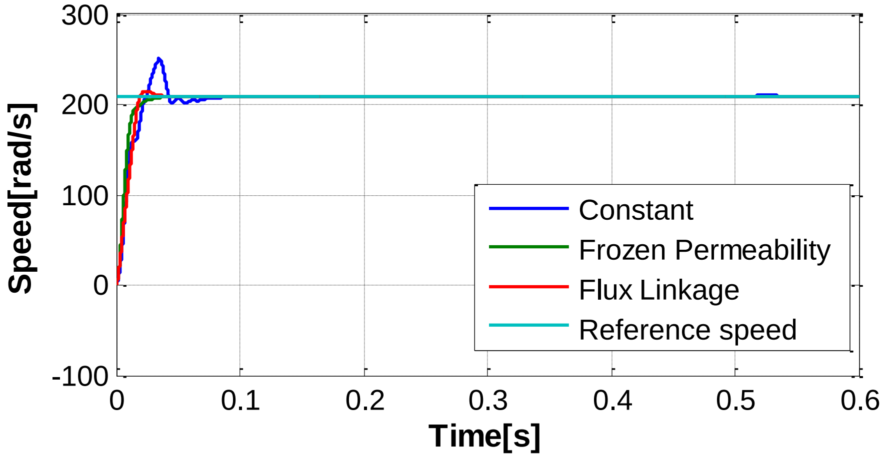

Figure 19. The speed of the PMSM

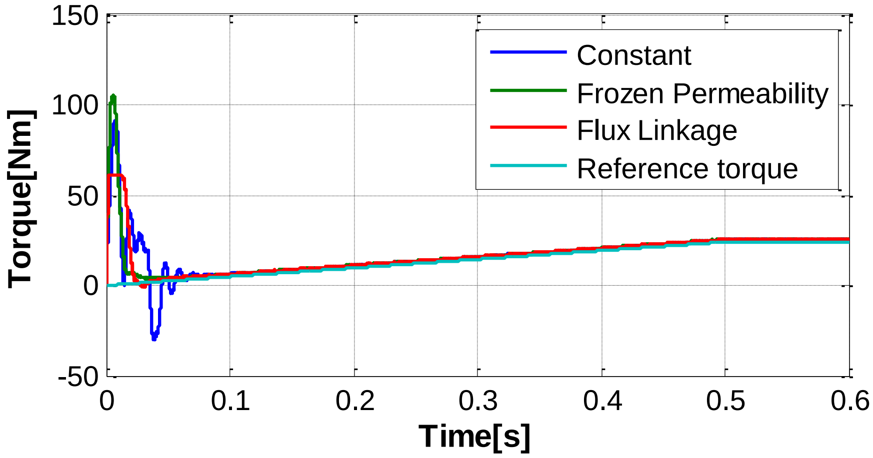

Figure 20. The electromagnetic torque of the PMSM

The higher the back emf, the lower the developed torque as shown in Figures 18 and 20. At start-up, it can be seen that frozen permeability model of the PMSM develops the highest torque. Its maximum values are close to the one obtained for the constant DQ inductances model. However, considering the saturation, in the flux linkage model the torque development is limited, which is normal as despite increased currents, the magnetic flux reaches its saturated values. During normal operation, the 3 models develop quite the same torque. A slight difference is noticeable. The flux linkage model's resulted torque is a little larger than the other two.

5. Development of the E-drive model in Simcenter AMESim using EMR

5.1. Simcenter AMESim Electric Motors and Drives (EMD) Library

Simcenter Amesim has an Electric Motors and Drives Library (EMD) library whose objective is to design for modelling electromechanical conversion subsystems, providing electrical and system engineers with a set of model components for electric machines and their control.
In the EMD library, mostly behavioural models are used. They are based on evaluation of look-up table characteristics, simple functional transfer functions or equivalent electrical circuits with various complexities.
Even though simulation time performance and accuracy can greatly depend on this modelling choice, the capabilities offered by the EMD library are compatible with multi-physics systems or subsystem analysis. The machine components especially consider electrical, mechanical and thermal quantity influences.

5.1.1. Library content

5.1.1.1. Category structure

The structure of the EMD library is shown in Figure 21. The components are sorted into subfolders according to the standard classification of electric machines:

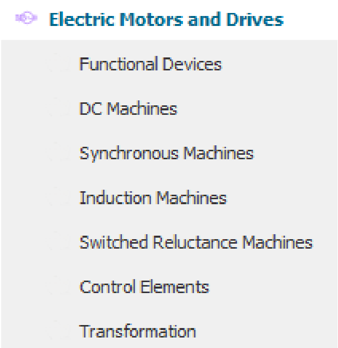

Figure 21. EMD library structure

The All repository contains a complete list of the EMD components (Figure 22):

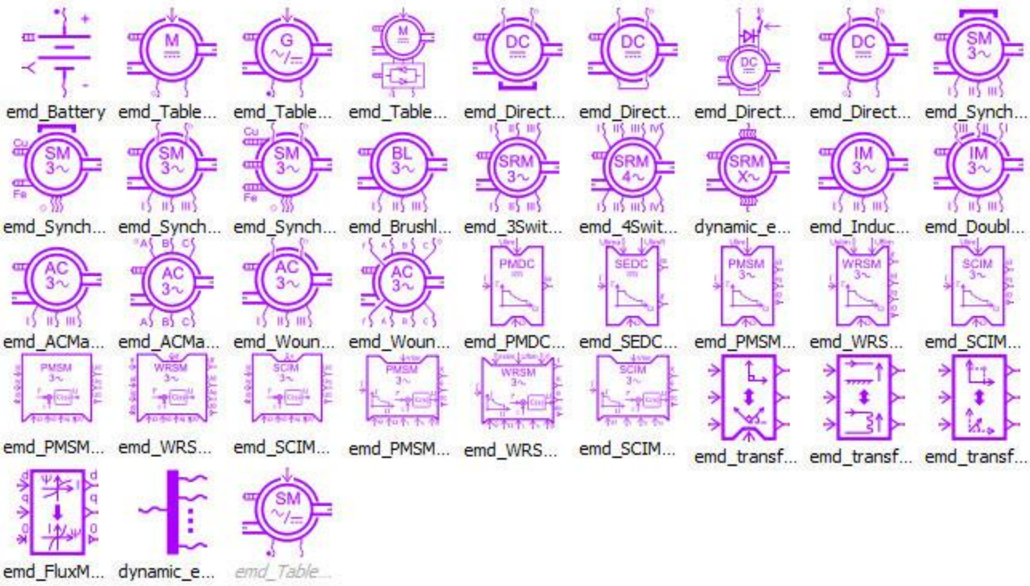

Figure 22. EMD library content

5.1.1.2. Notations and conventions

5.1.1.2.1. Electrical conventions: dipoles

The passive and active sign conventions for dipoles are represented in Table 2:

Table 2. Electrical convention for current and voltage

Passive convention	Active Convention
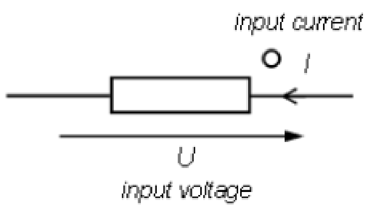	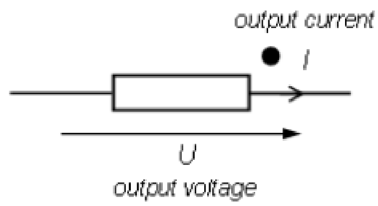

Both conventions are used in EMD. For example, electric machine phases are considered to take power from the circuit and use the passive sign convention, indicated on the icons with a white dot. On the other hand, generator phases are considered to give power to the circuit and use the active sign convention, indicated on the icon with a dark dot. Examples of icons for both cases are given in Figure 23:

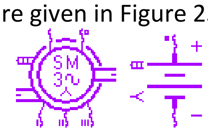

Figure 23. EMD icons with passive (white dot) and active (dark dot) sign convention

For both the machine and the battery, the power exchanged with the circuit can be positive or negative since these devices are reversible. However, the dot on the icon indicates the type of convention used and the direction of the voltage and current quantities:

- Submodels using the passive sign convention have input voltage and input current variables as represented in Table 2. The product of these quantities is an instantaneous power, positive if energy is going into the model.
- Submodels using the active sign convention have output voltage and output current variables as represented in Table 2. The product of these quantities is a power, positive if energy is going out of the model.

5.1.1.2.2. Electrical conventions: three phase windings

Three-phase machines only have three electrical ports since the windings are connected in a star or delta connection. The electrical ports are associated on icons with the symbols I, II and III.
The equivalent windings in the three-phase machine are called A, B and C.
The winding connection, the current and voltage direction and relationship with the electrical ports are summarized in Table 3:

Table 3: Winding connection and electrical convention for three-phase machines

<table>
<tr><th>Star (or Y) connection</th><th>Delta (or Triangle) connection</th></tr>
<tr><td>
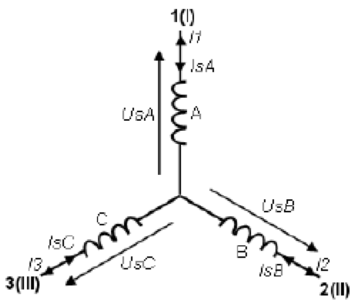

</td><td>
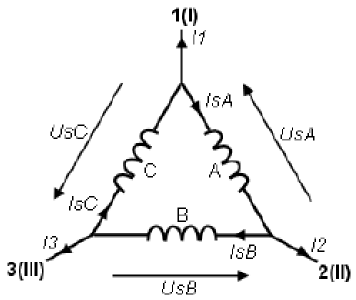

</td></tr>
</table>

5.1.1.2.3. Electrical conventions: electrical angle

Stator phase A is the reference for the stator. Either rotor phase A or the field phase is the reference for the rotor. The electrical angle is then the angle between the stator and the rotor references.
Moreover for three phase AC machines, the windings order is A, B, C and they have an electrical phase lag of $2\pi/3$ rad with each other. If we set a constant magnetic field in the machine rotor for example and put it in motion so that the electrical angle rises, a back electromotive force will be created in the stator phases. The rotation will indeed create a variation of the stator phase flux linkages. Then the back electromotive force created in the A phase when the electrical angle is 0 rad will be the same as the back electromotive force created in the B phase when the electrical angle is $2\pi/3$ rad.
The electrical angle and the winding position for the stator can be summed up in Figure 24:

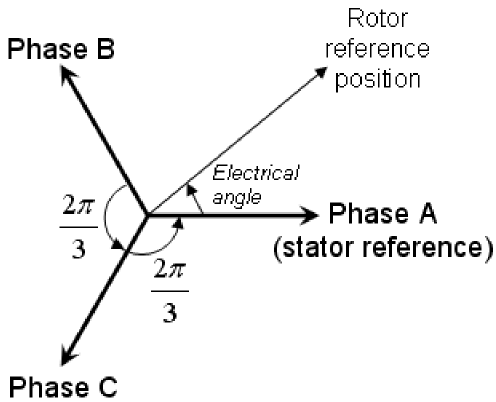

Figure 24. Electrical angle definition

5.1.1.2.4. Space phasor definition

Balanced three-phase AC systems can be represented with space phasor quantities for both line current and line-to-neutral voltage. Space phasors are defined by RMS magnitude and phase angle.
The angles are defined relative to a reference rotating frame (Figure 25):

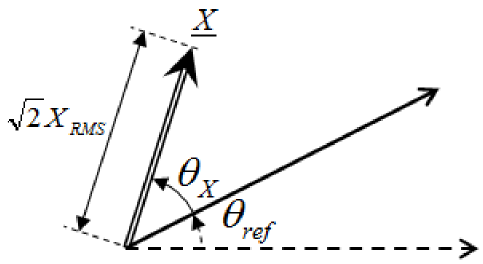

Figure 25. Space phasor representation

The reference frame angle and frequency are algebraic quantities, positive in the anticlockwise direction.
The direction definition of the current space phasor at ports is identified with their causality.
The current and voltage phase angle are defined relative to the reference frame and are positive in the anticlockwise direction.

5.1.1.2.5. Mechanical convention

An electric machine is reversible; it can work either as a motor or as a generator.
Using the motor convention, the rotor relative speed can be measured with *W as* an output speed at the mechanical port and the electromagnetic torque can be measured with *T* as an output torque at the mechanical port. The mechanical power exchange of an electric machine with rotary velocity *W*, torque *T* and output mechanical power *Pm* is summarized in Figure 26:

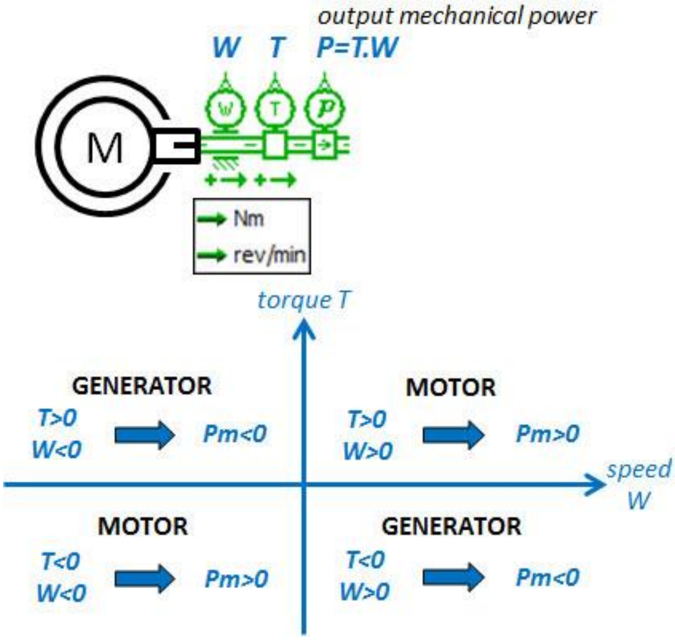

Figure 26. The mechanical convention definition

When *W* and *T* are of the same sign, the machine is working as a motor and the output mechanical power *P* is positive.
When *W* and *T* are of opposite sign, the machine is working as a generator and the output mechanical power *P* is negative.

5.2. EMR-based e-drive in Simcenter AMESim

The philosophy of testing a preliminary model in Simcenter AMESim was to compare the outputs of the machine under test (PMSM) with a corresponding machine that is certified to be operational in the Simcenter AMESim Library. The latter one was a DC machine. The interest is not at all focused on the DC machine, but on the PMSM.

The DC machine is just a quide reference for the mechanical behavior of the PMSM. A first EMR library has been recently developed in Simcenter AMESim for the PANDA project [Husar 2019].

The actions necessary for integrating a permanent magnet synchronous machine (PMSM) on an electric vehicle (EV) model, in simulation, are presented.
An electric vehicle model using a quasi-static battery model and a DC machine with a chopper, is available. The DC machine and the chopper are to be replaced by a PMSM and an inverter developed in WP3. All the other vehicle components will remain the same
The PMSM model based on the collaboration between WP3 and WP4, represent the first PANDA EMR e-drive model simulated within Simcenter AMESim. The model developed in section 3 will be implemented in the EMR-based library of Simcenter AMESim. Thus, we will have two different e-drive models that, depending on the level of simulation can be used (multi-level knowledge model).
As an objective, component integration implies direct connection and should be done with ease.

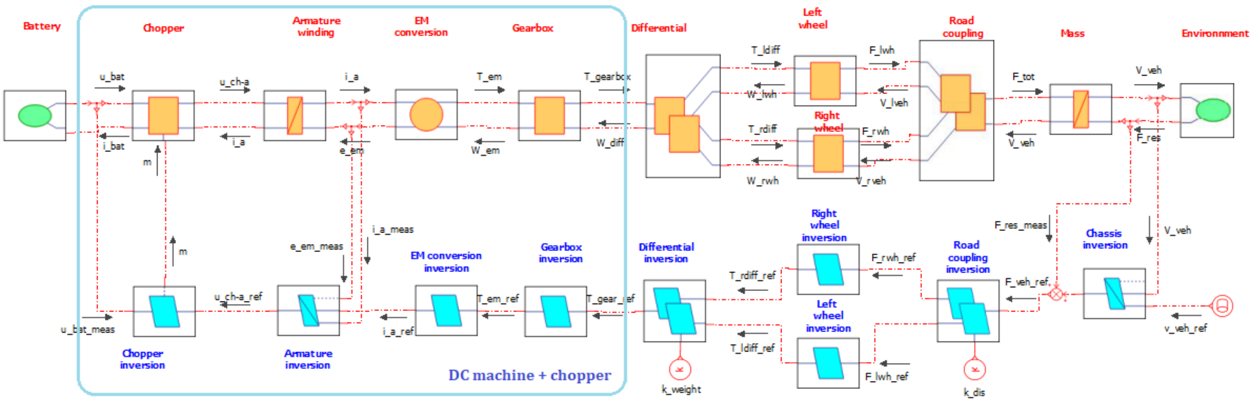

Figure 27. DC machine integrated in the EV model [Husar 2019]

To facilitate machine integration, the boundaries of the component and the interconnection variables are determined.
The inverter is connected directly to the PMSM through one of their two ports. The inverter should connect, at the other port, with the battery through the electric variables: battery current i_{bat} and voltage u_{bat}.
The PMSM should connect, at the other port, with the gearbox. The interconnection variables are: rotor torque T_{sm} and rotor angular velocity $\delta\omega$.

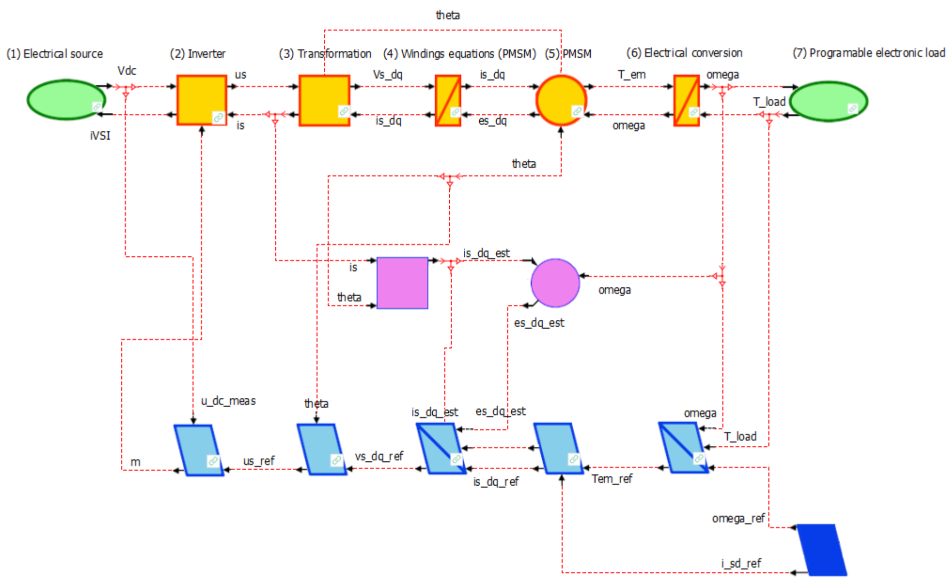

Figure 28. PMSM machine to be connected

The control components in EMR could also be transferred easily because of the symmetric layout of the EMR with inversion-based control, and the fact that the controllers used are local. Thus, the controllers corresponding to all the EMR elements selected is transferred. The estimation elements is also included.
With these boundaries fixed, the electric machine module is defined, which can be easily integrated indifferent of its type, i.e. DC or AC, including its control system.
The direct connection of the PMSM and the inverter to the EV simulation in place of the chopper and the DC machine, is done successfully. The interaction at the boundary match, all required information through the interconnections being provided (Figure 29).

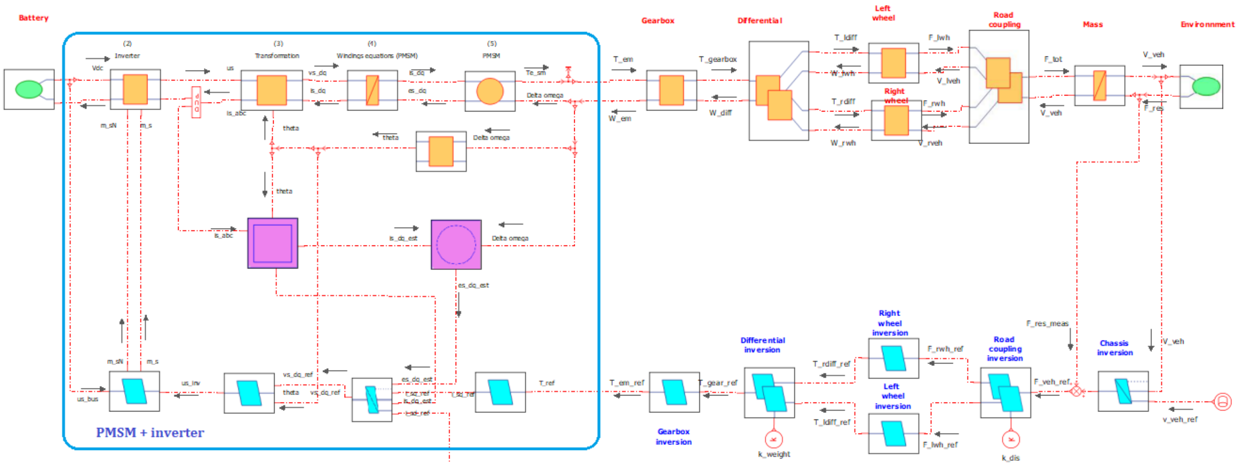

Figure 29. PMSM integrated in the EV model

The simulation run parameters are set as shown in the table below and the integrator type is set to standard integrator.

Simulation settings

Parameter	Value	Unit
Start time	**10.99**	s
Final time	**11.3**	s
Print interval	**1e-6**	s

A simulation run results in failure, as some of the system variables become unexpectedly large, while the measured vehicle velocity is at zero. The fast-growing variables are indicating system instability (Figure 30).

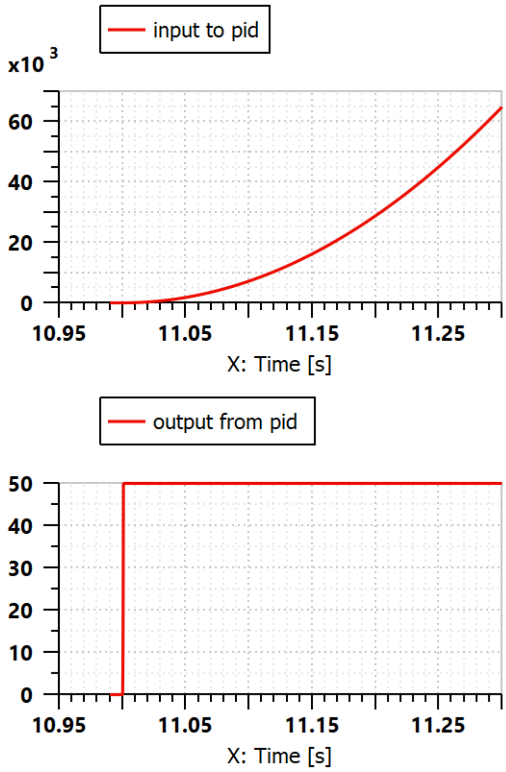

Figure 30. PID input and output for reference signal $i_{sq,ref}$

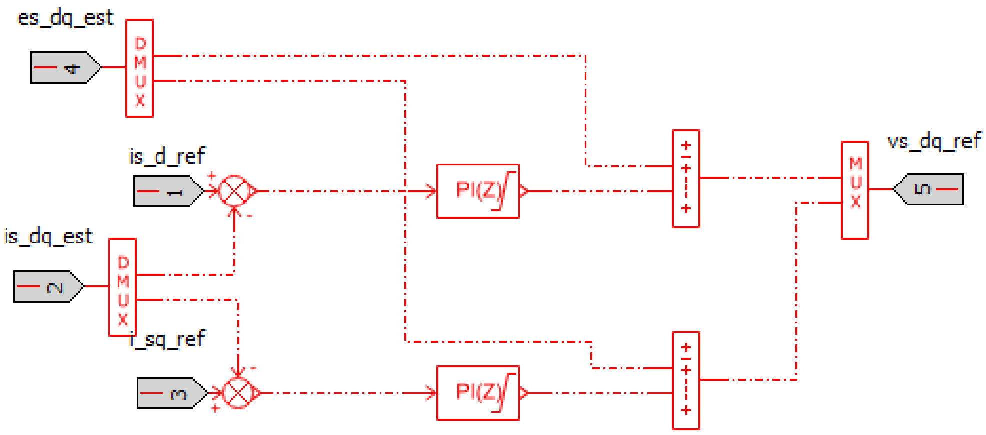

Figure 31. Closed-loop current controller

The cause of instability was found to be the wind-up effect, due to current-controller saturations (Figure 31). The saturation limits are set as in the table below.

Title	Value	Unit	Tags	Name
integral part	0	null		ipart
controller type	**PI**			outputtype
integration method	forward Euler			method
limit output	**yes**			outlim
anti windup method	stop integration			antiwind
proportional gain	**kp_pmsm**	null		Kp
integral gain	**ki_pmsm**	null		Ki
backtracking gain	0	null		Ks
sample period	**Ts**	s		period
minimum permitted output value	**-50**	null		outmin
maximum permitted output value	**50**	null		outmax

The solution was to set the saturation limits large enough such that saturation does not occur. Making this change, will turn the system stable, by allowing the controllers to provide appropriate (bounded) commands to the plant (Figure 32).

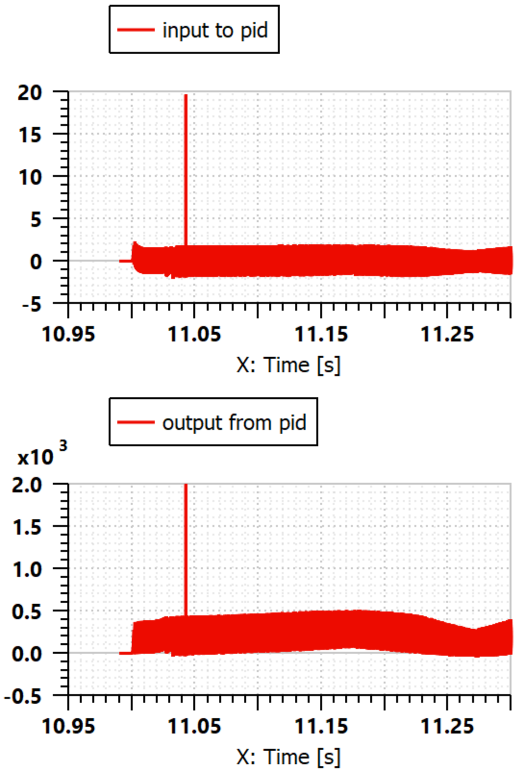

Figure 32. PID input and output for reference signal $i_{sq,ref}$ and saturation limits

As a result, the simulation run successfully, making available, for processing and analysis, the simulation system variables, in stable system operation.
Simulation results (in Figure 33) show that the measured vehicle velocity using the PMSM is indistinguishable from the measured vehicle velocity using the DCM, which can closely track the NEDC (New European Driving Cycle) reference. This indicates that the PMSM runs correctly, and the controllers keep the system stable while vehicle reference tracking is achieved.

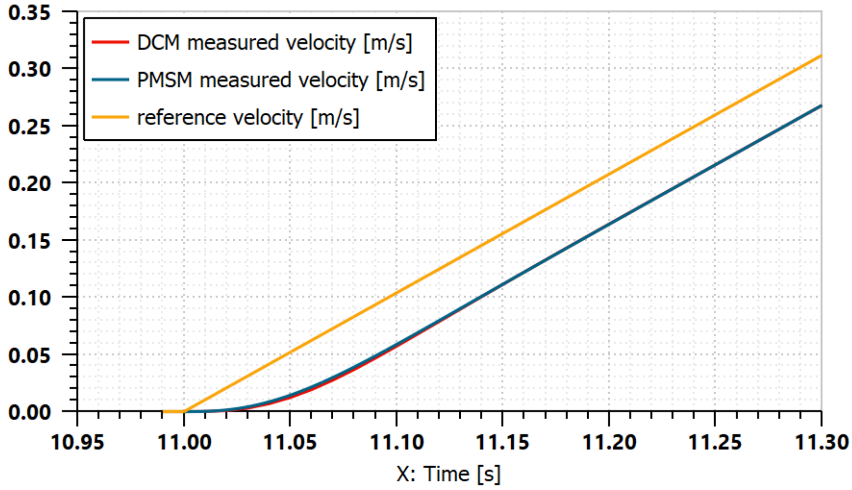

Figure 33. Measured vehicle velocity comparison between PMSM and DCM

To illustrate the comparison between the two types of motors, the rotor torque is plotted in Figure 34, where the matching between the variables is visible. Again, this indicates correct operation of the PMSM in simulation.

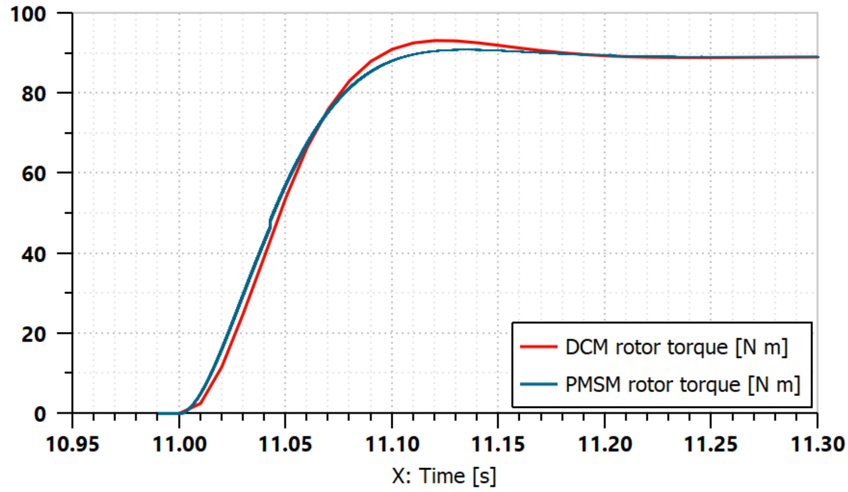

Figure 34. Rotor torque comparison between the PMSM and DCM.

A characteristic of PMSM, in simulation, is the presence of signal chattering, i.e. high frequency harmonics of small amplitude. The behavior in the torque signal is presented in Figure 35.

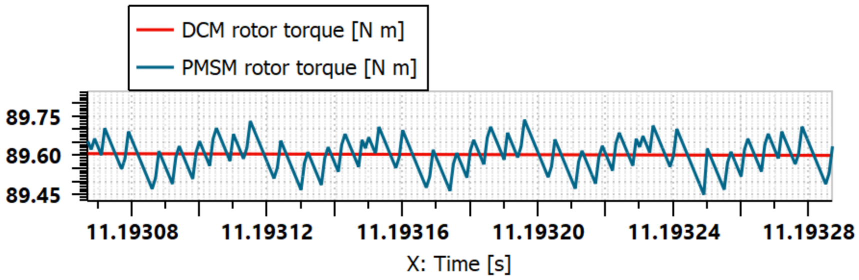

Figure 35. Torque chattering

The small amplitude of the high frequency harmonics does not affect the overall system behavior, as the high amplitude components of the signal are such that desired vehicle velocity is achieved.

The PMSM integration process in the EV EMR diagram was demonstrated and a comparison of the EV model using a PMSM with an EV model using a DC machine was made.
This PMSM integration would help to assess the state of the simulation model and the resulting EV simulation could thus be used for EV design and development.

6. Conclusions and future work

The presented report, multi-level modelling of an AC machine provides a detailed positioning of the project PANDA. Therefore, different models have been proposed from the most accurate to the simple one for the study of the AC machine. Also, according to PANDA methodology the models were organised using EMR.
Because all the models will be integrated in Simecenter AMESim software, an introduction regarding the analogy of simulation models from MATLAB/Simulink to Simecenter AMESim was performed using the EMR library developed in PANDA.

The team of UTCN developed PMSM multi-level models based on data and hardware that are at their disposal. This data regards detailed information about the machine's architecture (lamination, materials, coils, winding, parameters, dimensions and mechanical characteristics). The laboratory of UTCN that is engaged in the PANDA project owns this particular machine, that will become in the future tasks part of the experimental test-bench for HiL validation of the project's models. Despite the initial requirements of creating self-excited synchronous machine models, the choice of creating permanent magnet synchronous ones was taken in order to build models that can be internally validated with existing hardware, justifying the feasibility of their work. However, the model designers are preparing simulation programs that will run also self excited machines. The transition from the PMSM models to the self-excited ones is quite simple and straight forward.

At the moment, the multi-level approach of the electrical machine is considered accomplished. The team focuses now on the multi-level analysis of the power inverter, developing models that will take into account switching losses and dead-time effects. This part of PANDA will be done by the team of UTCN during task 3.2. The latter is justified by the fact that at UTCN there is an ongoing building process of a test-power inverter that will be refence for creation of the multi-level inverter models but in a behavioral approach. These models will be directly validated by measured quantities comparing those with ones obtained simulation wise. At this level, a complete simulation of the multi-level electrical machine with the multi-level inverter models will be ready for testing. Going further, in task 3.3 the HiL testing of the earlier simulated entities will be approached, coupling the machine already existing with the power inverter, now under development. This validation philosophy allows UTCN to prove the feasibility of their model. HiL testing for actual larger power motors and inverters from PANDA project will be straight forward requiring only hardware data information to be uploaded into the actual simulation models.
In doing so UTCN can develop their models, offer reliable validation and in the same time prepare them for testing the actual PANDA hardware as required.

7. Deviations

No deviations with respect to the description of work.

8. References

[Bobek 2005] V. Bobek, “PMSM Electrical Parameters Measurement”, Freescale Semiconductor, Inc., 2013

[Bouscayrol 2012] A. Bouscayrol, J. P. Hautier, B. Lemaire-Semail, "Graphic Formalisms for the Control of Multi-Physical Energetic Systems", Systemic Design Methodologies for Electrical Energy, tome 1, Analysis, Synthesis and Management, Chapter 3, ISTE Willey editions, October 2012, ISBN: 9781848213883

[Bouscayrol 2005] A. Bouscayrol, P. Delarue, and X. Guillaud, “Power strategies for maximum control structure of a wind energy conversion system with a synchronous machine,” Renew. Energy, vol. 30, no. 15, pp. 2273–2288, May 2005

[Ciornei 2019] S. M. Ciornei, M. Ruba, R. O. Nemes, C. Husar and C. Martis, "Modeling. control and simulation of a light electric vehicle propulsion system based on EMR," 2019 AEIT International Annual Conference (AEIT), Florence, Italy, 2019, pp. 1-6.

[Dealrue 2003] P. Delarue, A. Bouscayrol, E. Semail, “Generic control method of multi-leg voltage-source-converters for fast practical implementation", IEEE Transaction on Power Electronics, vol. 18, no. 2, pp. 517-526, March 2003

[Drobnic 2019] K. Drobnic, L. Gasparin, R. Fiser, “Fast and AccurateModel of Interior Permanent-Magnet Machine for Dynamic Characterization”, Energies, 2019.

[EMR 2019] “EMR web site”, http://www.emrwebsite.org/ [Online] [Consulted: November 2019].

[Husar 2019] C. Husar, M. Grovu, C. Irimia, A. Desreveaux, A. Bouscayrol, M. Ponchant, P. Magnin, “Comparison of Energetic Macroscopic Representation and structural representation on EV simulation under Simcenter Amesim”, IEEE-VPPC’19, Hanoi (Vitenam), October 2019 (Siemens Software and L2EP Within the framework of the H2020 PANDA project).

[LHomme 2012] W. Lhomme, P. Delarue, F. Giraud, B. Lemaire-Semail and A. Bouscayrol, "Simulation of a Photovoltaic Conversion System using Energetic Macroscopic Representation," 2012 15th International Power Electronics and Motion Control Conference (EPE/PEMC), Novi Sad, 2012.

[Nemes 2019] R. O. Nemes, S. M. Ciornei, M. Ruba and C. Martis, “Real-time simulation of scaled propulsion unit for light electric vehicles”, Electrical Engineer, Spinger Nature, 2019.

[Pinto 2017] D. E. Pinto, A. C. Pop, J. Kempkes, J. Gyselinck, “dq0-Modeling of Interior Permanent-Magnet Synchronous Machines for High-Fidelity Model Order Reduction, Optim & Intl Aegean Conference on Electrical Machines and Power Electronics, May, 2017.

[Yucelen 2016] T. Yucelen, O. Kaymakci and S. Kurtulan, “Self-Tuning PID Controller Using Ziegler-Nichols Method for Programmable Logic Controllers”, Electrical and Electronic Faculty, Istanbul Technical University, Maslak, Istanbul, Turkey, 2016.

[Zarko 2005] D. Zarko, D. Ban, R. Klaric, “Finite Element Approach to Calculation of Parameters of an Interior Permanent Magnet Motor”, Automatika 46, 2005.

Appendix A – Project Partners

The objective of the project PANDA is to provide a disruptive and open access model organization for an easy interconnection and change of models in the development process of EVs. In that aims, it is composed of academic and industrial partners.

Table 4: Project Partners

#	Type	Partner	Partner Full Name
1	UNIV	ULille	Université de Lille
2	IND	SISW	Siemens Industry Software SRL
3	UNIV	VUB	Vrije Universiteit Brussels
4	IND	VEEM	VALEO Equipement Electriques Moteur SAS
5	UNIV	UTCN	Universitatea Tehnica Cluj Napoca
6	SME	TY	Tajfun HIL (Typhoon HIL)
7	IND	TUV	TUV SUD AG
8	UNIV	UBFC	Université Bourgogne Franche-Comté
9	SME	UNR	Uniresearch BV
10	IND	RTR	Renault Technologie Roumanie
11	SME	Bluways	BlueWays International bva

This project has received funding from the European Union's Horizon2020 research and innovation programme under Grant Agreement no. 824256.

Appendix B – EMR graphical pictogram

Table 5: EMR pictogram [Bouscayrol 2012]

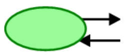	Source element (energy source)	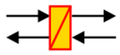	Accumulation element (energy storage)	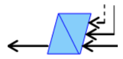	Indirect inversion (closed-loop control)
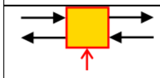	Mono-physical conversion element	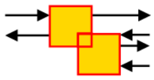	Mono-physical coupling element (energy distribution)	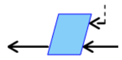	Direct inversion (open-loop control)
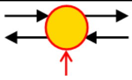	Multi-physical conversion element	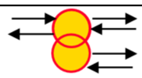	Multi-physical coupling element (energy distribution)	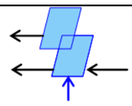	Coupling inversion (energy criteria)

Appendix C - Abbreviations

BEV- Battery electric vehicle
EMR- Energetic macroscopic representation
FEA- Finite element analysis
FEM- Finite element method
FCV- Fuell cell vehicle
FLM- Flux linkage model
FOC- Field oriented control
P-HEV- Plug-in hybrid electric vehicle
PMSM- Permanent magnet synchronous machine
SPWM- Sinusoidal pulse width modulation
VSI- Voltage source inverter